

# Harmonic Frequency Locking in the Multifrequency Recirculating Planar Magnetron

Geoffrey B. Greening<sup>1</sup>, Member, IEEE, Steven C. Exelby<sup>2</sup>, Student Member, IEEE, Drew A. Packard, Student Member, IEEE, Nicholas M. Jordan<sup>3</sup>, Member, IEEE, Y. Y. Lau, Fellow, IEEE, and Ronald M. Gilgenbach, Life Fellow, IEEE

**Abstract**—This paper presents experimental results that demonstrate the first known instance of harmonic frequency locking in a magnetron. The prototype crossed-field high-power microwave source, termed the multifrequency recirculating planar magnetron, consisted of two planar cavity arrays having design frequencies near 1 and 2 GHz, respectively, coupled by smooth-bore electron beam recirculation bends. The magnetron was driven by the MELBA-C modified Marx generator using  $-300$ -kV pulses supplying up to 3 kA for approximately 300 ns. Using a 0.17-T axial magnetic field, the harmonic frequency-locked state simultaneously produced microwave pulses of  $32 \pm 3$  MW at  $0.984 \pm 0.001$  GHz and  $13 \pm 2$  MW at  $1.970 \pm 0.002$  GHz. In addition, changes in the relative phase difference between the magnetron slow wave structures (SWSs) were correlated with changes in the axial magnetic field magnitude. This correlation, along with the results from experiments that tested each individual planar cavity array in isolation, suggested the locking was facilitated through the second harmonic content of the 1-GHz modulated electron beam recirculating from the 1-to-2-GHz SWS. Analysis of shots conducted near 0.17 T showed a  $\pm 17^\circ$  shot-to-shot variation in the average relative phase difference between the SWSs, and the average variation in this phase difference during a locked shot was  $\pm 8^\circ$ .

**Index Terms**—Frequency harmonics, frequency locking, high-power microwave (HPM) generation, magnetrons, microwave oscillators, vacuum electronics.

Manuscript received October 31, 2017; revised February 17, 2018; accepted February 22, 2018. Date of publication March 26, 2018; date of current version May 21, 2018. This work was supported in part by the Office of Naval Research under Grant N00014-13-1-0566 and Grant N00014-16-1-2353 and in part by L-3 Communications Electron Devices. The work of G. B. Greening, S. C. Exelby, and D. A. Packard supported by the Directed Energy Professional Society. The review of this paper was arranged by Editor D. K. Abe. (Corresponding author: Geoffrey B. Greening.)

G. B. Greening was with the Plasma, Pulsed Power, and Microwave Laboratory, University of Michigan, Ann Arbor, MI 48109 USA. He is now with Communications and Power Industries, Beverly Microwave Division, Beverly, MA 01915 USA (e-mail: geofgree@umich.edu).

S. C. Exelby, D. A. Packard, N. M. Jordan, Y. Y. Lau, and R. M. Gilgenbach are with the Plasma, Pulsed Power, and Microwave Laboratory, University of Michigan, Ann Arbor, MI 48109 USA (e-mail: srexlb@umich.edu; drupac@umich.edu; jordann@umich.edu; yylau@umich.edu; rongilig@umich.edu).

Color versions of one or more of the figures in this paper are available online at <http://ieeexplore.ieee.org>.

Digital Object Identifier 10.1109/TED.2018.2810240

## I. INTRODUCTION

MAGNETRONS are powerful, compact, efficient RF sources with applications in industry, science, and defense [1]–[3]. Magnetrons have also been demonstrated as a high-power microwave (HPM) source [4]–[6], although the range of frequencies that can be produced using a single magnetron is relatively limited because they are inherently narrowband devices. Several methods have been developed to expand the range of frequencies that can be produced using a single magnetron, including mechanical tuning and operation in different resonant electromagnetic modes [7]–[9]. Magnetrons have also been the subject of many oscillator locking studies, including both master–slave and peer-to-peer configurations for both conventional and relativistic magnetrons [10]–[16].

Recently, the multifrequency recirculating planar magnetron (RPM) [MFRPM, Fig. 1(b)] demonstrated simultaneous HPM generation near both 1 and 2 GHz using two planar slow wave structures (SWSs) having different design frequencies coupled by smooth-bore cylindrical bends that recirculate the electron beam from each SWS to the other [17]. The MFRPM design was a variant of the single-frequency RPM, which utilized two identical, planar SWSs [18]–[21].

Since the single-frequency RPM experimentally demonstrated frequency locking between its two planar oscillators [20], the MFRPM was designed to determine whether an analogous locking phenomenon would occur between two structures related by a frequency harmonic, where the frequency of the second oscillator would lock exactly to the second harmonic of the first oscillator. Initial experiments using the MFRPM did not demonstrate any locking behavior [17]. Further investigation determined that the absence of cylindrical symmetry in the MFRPM resulted in location-dependent magnetic field diffusion times, since the magnetic field must diffuse into the structure from pulsed electromagnets located outside the magnetron. An optimization of trigger delay times corrected the field asymmetry, which led to the successful demonstration of a harmonic frequency-locked state in the MFRPM. This paper characterizes the locked state, which is the first known instance of harmonic frequency locking in a magnetron.

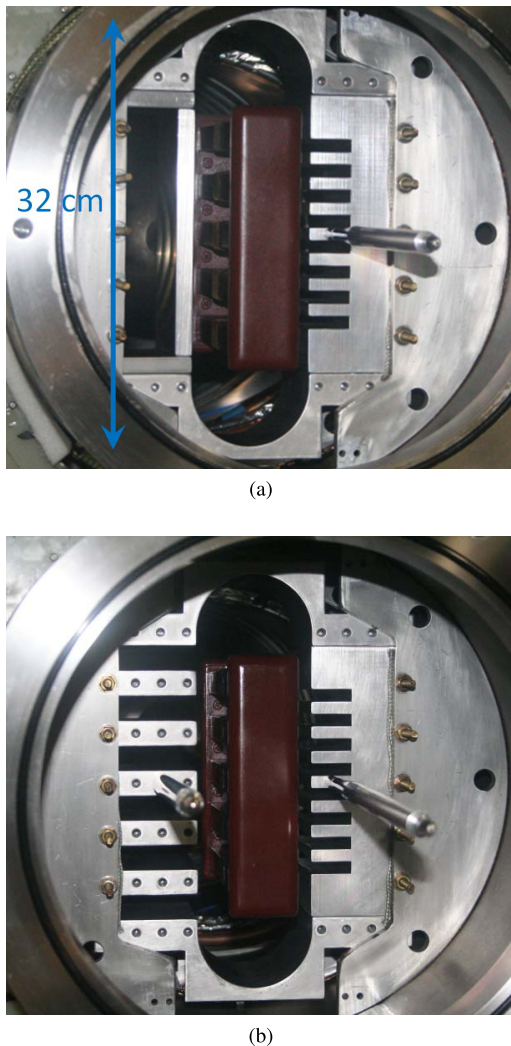


Fig. 1. Photographs of two magnetron anode configurations. Photographs of the (a) isolated SBO configuration in the MELBA-C vacuum chamber and (b) MFRPM configuration in the MELBA-C vacuum chamber.

The experimental configuration is first described, followed by a summary of the experimental results. A detailed analysis and discussion of the harmonic frequency-locked state follows, and the final section offers concluding remarks on potential areas for future study.

## II. EXPERIMENTAL CONFIGURATIONS

The MFRPM anode consisted of a 1 GHz, six-cavity SWS (termed the L-band oscillator, LBO) and a 2 GHz, eight-cavity SWS (termed the S-band oscillator, SBO), each of which was designed to operate in the  $\pi$ -mode (characterized by a  $180^\circ$  phase advance per cavity) and had a 2.6-cm anode-cathode gap spacing. These two oscillators were coupled by smooth-bore recirculation bends and shared a common cathode. A detailed description of the design can be found in [17] and [22]. Characterization of each individual oscillator was performed using two separate, isolated anode configurations in which one of the oscillators was replaced using a linear, smooth drift region. Fig. 1 shows two photographs (a) an isolated configuration (SBO) and (b) the full MFRPM anode.

Fig. 2 illustrates the experimental configuration. A pulsed voltage ( $-300$  kV, 200–400 ns) was applied to the cathode (termed the second mode control cathode [20], [23]) using the Michigan electron long beam accelerator with Ceramic insulator (MELBA-C), and the magnetron typically drew 1–3 kA at peak microwave output power, depending on the anode configuration. The cathode included endcaps to reduce axial current losses, although the recirculation bends remained uncovered and likely resulted in considerable endloss current as evidenced by material erosion axially downstream from the bends. Microwaves were extracted from the center vane of each oscillator and coupled into coaxial transmission lines using antennas. This axial extraction technique was a relatively straightforward implementation that could be applied within the limits of existing hardware and was not optimized for maximum power extraction. The coax lines were then adapted to WR-650 and WR-340 waveguide for the LBO and SBO, respectively. Microwaves were sampled using waveguide loop directional couplers, and each waveguide was terminated using matched loads. In the isolated anode configurations, the microwave antenna was omitted for the oscillator that was replaced using the smooth drift region; all other components were unchanged. The base pressure was approximately  $1 \mu\text{torr}$  for all tested configurations. An axial magnetic field was imposed on the structure using two pulsed electromagnets in a pseudo-Helmholtz configuration centered on the anode. Field magnitudes were between 0.1 and 0.3 T.

The sampled microwave signal from each directional coupler was split into two channels using 3-dB power dividers. The first channel was recorded directly using a fast Agilent 54855A oscilloscope (20 Gsamples/s), and the second channel was fed to calibrated Agilent 8472B low-barrier Schottky diodes for power measurements captured using a Tektronix 3054 oscilloscope. Attenuation of all components (directional couplers, cables, splitters, and attenuators) was determined at the design frequencies of the two oscillators. The magnetron current was determined using time-integrated Rogowski coil signals, and the operating voltage was measured using a  $\text{CuSO}_4$  voltage divider. Both diagnostics were captured using the Tektronix oscilloscope.

## III. EXPERIMENTAL RESULTS

Each SWS was tested individually using the isolated anode configurations to establish an operating baseline for each design. In Section II, these data are compared to results obtained using the MFRPM anode configuration to understand what operational changes was exhibited by the LBO and SBO when run concurrently.

### A. Results for the Isolated LBO and SBO Anodes

Baseline results for the isolated LBO and SBO are summarized in Tables I and II, respectively. Both anodes demonstrated optimal power production near  $B = 0.16$  T, which agrees with the Buneman–Hartree condition for synchronous beam-wave interaction ( $B_{\text{BH}} = 0.158$  T at 300 kV). Note that the isolated LBO also exhibited high microwave powers at higher magnetic fields near  $B \simeq 0.23$  T [22], although this range falls outside the region of interest for this paper.

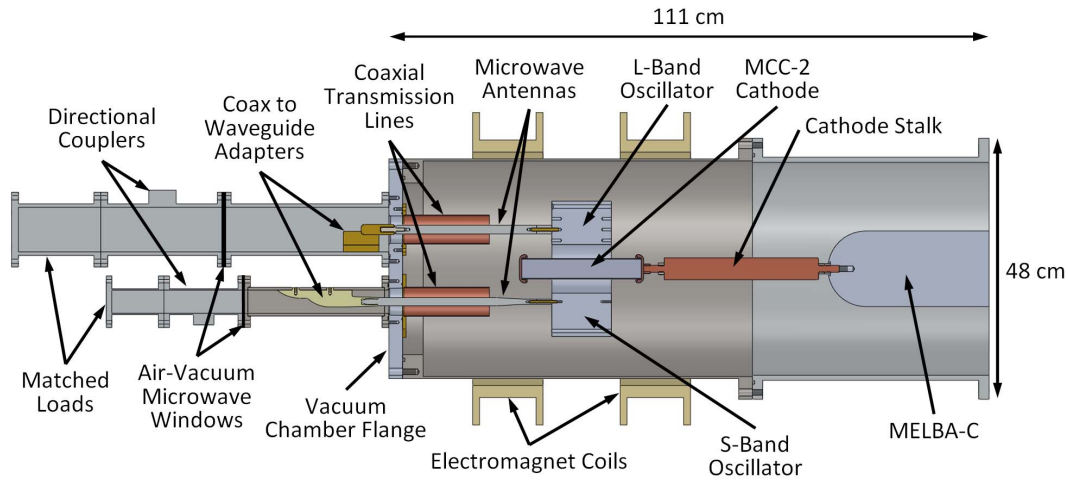


Fig. 2. Top sectional diagram of the MELBA-C vacuum chamber and MFRPM components. The anode support structure is not shown.

TABLE I

SUMMARIZED PERFORMANCE METRICS FOR THE ISOLATED LBO NEAR  $B = 0.16$  T

$\pi$ -Mode Power [MW]:	25	$\pm$ 2
$\pi$ -Mode Frequency [MHz]:	986	$\pm$ 3
Impedance [ $\Omega$ ]:	124	$\pm$ 8
Efficiency [%]:	5	$\pm$ 1

TABLE II

SUMMARIZED PERFORMANCE METRICS FOR THE ISOLATED SBO NEAR  $B = 0.16$  T

$\pi$ -Mode Power [MW]:	18	$\pm$ 2
$\pi$ -Mode Frequency [MHz]:	2022	$\pm$ 4
Impedance [ $\Omega$ ]:	236	$\pm$ 21
Efficiency [%]:	7	$\pm$ 2

Several important observations resulted from these experiments. First, the free-running  $\pi$ -mode frequency of the SBO was not precisely twice the frequency of the free-running  $\pi$ -mode frequency of the LBO. Were this the case, the frequency of the SBO  $\pi$ -mode ought to fall near 1.97 GHz instead of 2.022 GHz. Second, mode competition was minimal near  $B = 0.16$  T, which suggested the  $\pi$ -mode was the preferred operating mode for both oscillators at the magnetic field corresponding to peak power production. Third, the frequencies of the other oscillator modes were experimentally identified as: 0.972 GHz (LBO  $5\pi/6$ -mode), 1.94 GHz (SBO  $6\pi/8$ -mode), and 2 GHz (SBO  $7\pi/8$ -mode). These frequencies were also in good agreement with both cold and hot tube simulations [22] conducted using HFSS [24] and MAGIC [25], respectively.

### B. Results for the MFRPM Anode

Results for the MFRPM anode are summarized in Table III for  $B = 0.16$ – $0.18$  T. This magnetic field range corresponded to the region of optimal operation, which was characterized by consistent production of high microwave powers and harmonic frequency locking between the LBO and SBO, although it

TABLE III

SUMMARIZED PERFORMANCE METRICS FOR THE MFRPM IN  $B = 0.16$ – $0.18$  T WHEREIN CONSISTENT FREQUENCY LOCKING OCCURRED

LBO $\pi$ -Mode Power [MW]:	32	$\pm$ 3
LBO $\pi$ -Mode Frequency [MHz]:	984	$\pm$ 1
SBO $6\pi/8$ -Mode Power [MW]:	13	$\pm$ 2
SBO $6\pi/8$ -Mode Frequency [MHz]:	1970	$\pm$ 2
Total Power [MW]:	40	$\pm$ 4
Peak Power $ \Delta t $ [ns]:	4	$\pm$ 3
Impedance [ $\Omega$ ]:	139	$\pm$ 7
Efficiency [%]:	10	$\pm$ 1

should be noted that the range over which locking occurred was broader ( $B = 0.14$ – $0.18$  T). These data will be discussed in detail.

Plots illustrating the voltage, current, microwave powers, and the time-integrated Fourier transforms for the LBO and SBO RF voltages are shown by Fig. 3 for a sample shot. The first plot [Fig. 3(a)] shows three features of note as follows.

- 1) The LBO was the first oscillator to start.
- 2) Both oscillators produced peak microwave powers with near simultaneity.
- 3) The microwave pulsewidth at half maximum power was approximately 20 ns.

These observations were generally true from shot to shot in  $B = 0.14$ – $0.18$  T. The second and third plots [Fig. 3(b) and (c)] show that, within uncertainty, the SBO frequency corresponded exactly to the second harmonic of the LBO. The combination of simultaneous peak power production and the harmonic frequency relation between the oscillators strongly suggests that the magnetron operated in a harmonic frequency-locked state wherein both oscillators behaved as a single, coupled device. This result represented a significant improvement over earlier results that were obtained prior to implementation of the trigger timing optimizations that substantially reduced magnetic field asymmetries [17].

Plots illustrating the aforementioned characteristics over the range of tested magnetic fields are shown in Fig. 4. As shown in Fig. 4(a), peak microwave power generation was consistent

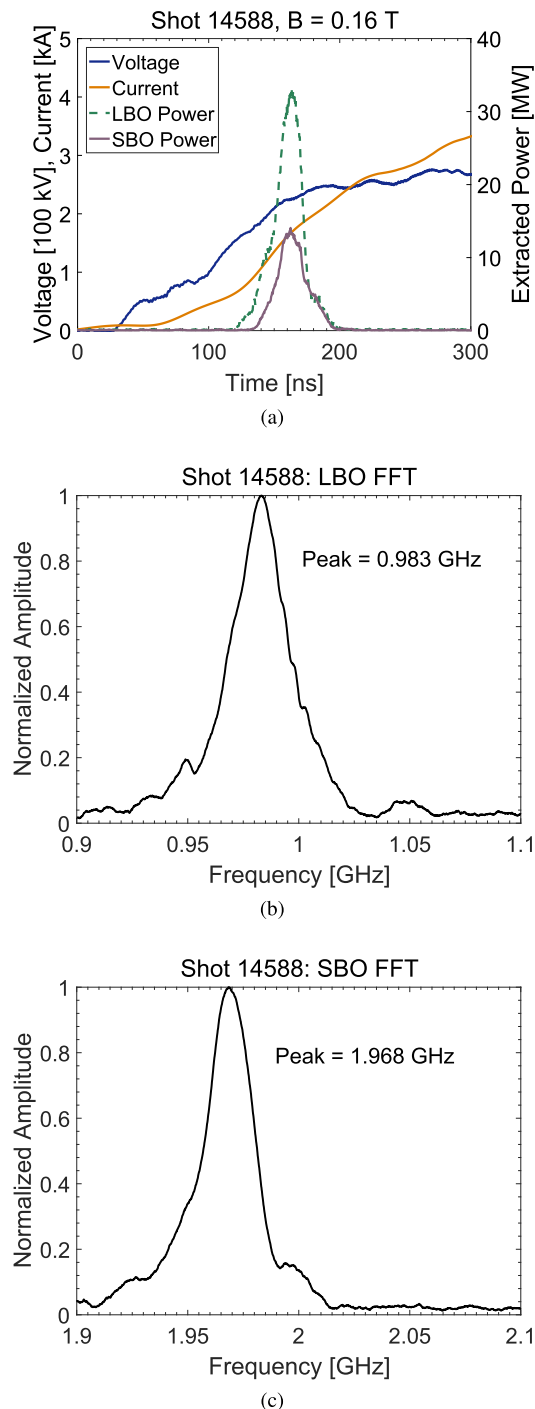


Fig. 3. Example of a harmonic frequency-locked shot conducted using the MFRPM anode and a 0.16-T axial magnetic field. (a) Plot of voltage, current, and RF power. Time-integrated Fourier transform of the (b) LBO RF voltage signal and (c) SBO RF voltage signal.

on a shot-to-shot basis in  $B = 0.14$ – $0.18$  T, whereas shots conducted at higher magnetic fields exhibited a considerable increase in shot-to-shot variability. Fig. 4(b) provides the strongest evidence of harmonic frequency locking between the structures, which clearly shows that the dominant SBO frequency was, within uncertainty, exactly twice the dominant frequency produced by the LBO. Furthermore, the aforementioned region of consistent power production corresponded to

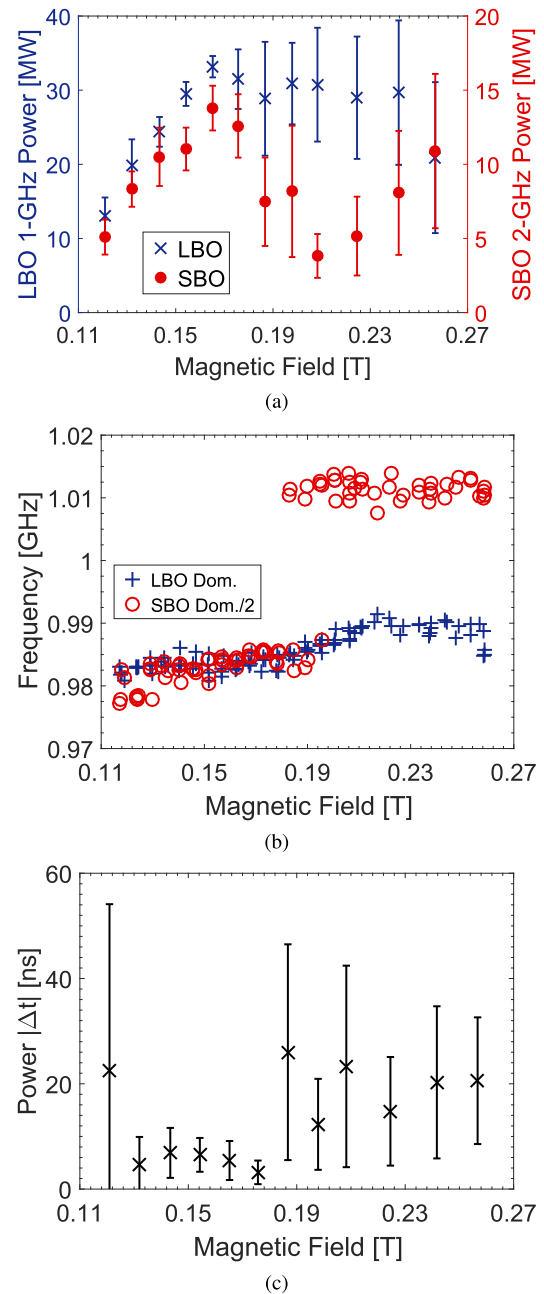


Fig. 4. Standard metrics for the MFRPM anode configuration. (a) Peak output powers for both oscillators versus magnetic field. Each point represents eight shots. The error bars indicate the standard deviation of each group of eight shots to illustrate the change in repeatability with magnetic field. (b) LBO dominant frequency and  $0.5 \times$  SBO dominant frequency versus magnetic field. (c) Absolute time difference  $|\Delta t|$  between oscillator peak powers versus magnetic field. Each point represents eight shots. The error bars indicate the standard deviation of each group of eight shots to illustrate the change in repeatability with magnetic field.

the same region in which harmonic frequency locking was observed. Finally, Fig. 4(c) shows that the two oscillators consistently produced peak power with near simultaneity in the harmonic frequency-locked region. In the plot, the peak power  $|\Delta t|$  is defined by  $|\Delta t| = |t_2 - t_1|$ , where  $t_1$  was the time at which peak power was observed from the LBO, and  $t_2$  was the time at which peak power was observed from the SBO.

#### IV. ANALYSIS OF THE HARMONIC FREQUENCY-LOCKED STATE

An in-depth analysis of the harmonic frequency-locked state was conducted to perform in the following.

- 1) Determine how the operation of each SWS differed between the locked state and the isolated, free-running configuration.
- 2) Identify a plausible locking mechanism.
- 3) Identify whether the locked state was a case of frequency locking (wherein the relative phase difference between the structures was random on a shot-to-shot basis) or phase locking (a more stringent condition wherein the relative phase difference was consistent from shot to shot [10]).

Comparison between LBO operation in Table III with Table I shows that, in the locked state, the LBO power increased from 25 to 32 MW, but the frequency did not change appreciably. This suggested the operating LBO mode in the locked state was the  $\pi$ -mode, as was the case in the isolated configuration at the same magnetic fields. A similar comparison for the SBO between Tables III and II shows that the SBO power was reduced from 18 to 13 MW, and that the frequency changed from 2.022 to 1.970 GHz. From these comparisons, it is clear that SBO operation was substantially different in the locked state relative to the isolated configuration, whereas the LBO was affected to a lesser degree.

As previously mentioned, the 1.970-GHz SBO frequency was not observed in the isolated configuration and did not correspond to any known mode. However, at the lowest magnetic fields tested, the SBO produced frequencies near the free-running  $6\pi/8$ -mode frequency on shots that did not demonstrate locking. Given the relatively close spacing between the second harmonic frequency of the LBO  $\pi$ -mode and the free-running SBO  $6\pi/8$ -mode frequency, it appears that the LBO, which consistently started first, primed the excitation of the SBO  $6\pi/8$ -mode and, through some locking mechanism, locked the SBO frequency to the exact LBO frequency harmonic (a frequency that differed slightly from the natural resonance of the  $6\pi/8$ -mode). This is particularly notable because the isolated SBO experiments demonstrated that the SBO naturally favored operation in the  $\pi$ -mode in  $B = 0.14$ – $0.18$  T, which suggests the locking mechanism was sufficiently strong to not only lock the frequency of the  $6\pi/8$ -mode OFF its natural resonance, but also excite the  $6\pi/8$ -mode over the naturally favored  $\pi$ -mode.

The locked state appeared to be a case of Adler-like master–slave locking because the SBO was strongly affected by the locked state, whereas the LBO was considerably less affected. While an Adler-like analytic model was developed to describe harmonic frequency locking [22], [26], a direct comparison with the experiment was not possible. However, some insight into the locking mechanism can be gained by investigating the relative phase difference between the SWSs. If the locking occurred through the electromagnetic fields, where the SBO structure fields coupled to the second harmonic of the LBO structure fields, the relative phase difference between the LBO and SBO should not be affected by changes in the electron beam velocity, which scales approximately

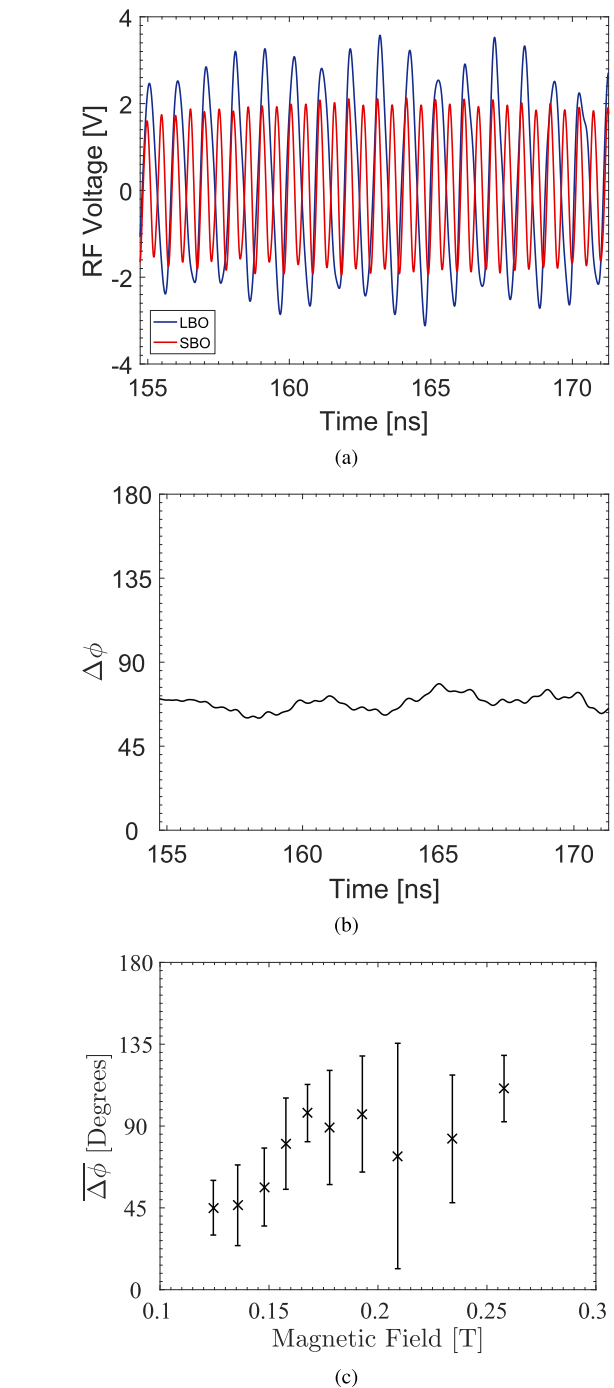


Fig. 5. Phase metrics for the MFRPM. (a) Splined and filtered RF voltage traces from both oscillators in the high-power time window. (b) Phase difference  $\Delta\phi$  between the oscillators in the high-power time window. (c) Mean phase differences  $\overline{\Delta\phi}$  and associated standard deviations of the means versus magnetic field. Frequency-locked operation occurred between 0.14 and 0.18 T.

as  $v_b \propto 1/B$ . Alternatively, if the locking occurred via the modulated electron beam exiting one SWS and entering the other, changes in the beam velocity should change the arrival time of the space charge bunches, thereby changing the relative phase difference between the SWSs. Thus, in addition to determining whether frequency locking or phase locking occurred, a phase analysis was conducted to also provide insight into the locking mechanism.

**TABLE IV**  
PHASE METRICS FOR THE MFRPM IN  $B = 0.16\text{--}0.17$  T  
ENCOMPASSING PEAK POWER PRODUCTION, WHEREIN  
CONSISTENT FREQUENCY LOCKING AND PREFERENTIAL  
SELECTION OF A RELATIVE PHASE  
DIFFERENCE OCCURRED

Phase Difference $\overline{\Delta\phi}$ [deg]:	93	$\pm$	17
Phase Variation $\overline{\sigma_{\Delta\phi}}$ [deg]:	8	$\pm$	4
Duration [ns]:	14	$\pm$	3

To determine the relative phase difference between the two SWSs, the RF voltage signals from each oscillator were first digitally processed to remove jitter and noise [27] and a processing time window was determined during which both oscillators were operating at powers  $\geq 67\%$  of their respective peak powers. Shots violating this condition were not considered in the phase analysis. An example of the RF traces for a locked case is shown in Fig. 5(a). The filtering process was thoroughly investigated to confirm that the original frequency and phase information remained unaffected. The phases of the signals were then extracted from their analytic representation, which was obtained using the Hilbert transform [28], [29]. After converting the phases to degrees, the LBO phase was multiplied by two to obtain its second harmonic, which was then subtracted from the SBO phase. For the previous RF voltage traces, the phase difference  $\Delta\phi$  is shown in Fig. 5(b). A representative phase difference  $\overline{\Delta\phi}$  for a shot was defined as the mean of the values of the phase difference within the processing window, and a measure of locking quality for each shot was defined as the standard deviation  $\sigma_{\Delta\phi}$  of the phase difference  $\Delta\phi$  in the respective processing windows of the shots. To avoid confusion between this quantity and standard deviations obtained for other plotted quantities, the standard deviation of the relative phase difference in the temporal processing window,  $\sigma_{\Delta\phi}$ , is termed the phase variation.

The representative phase difference  $\overline{\Delta\phi}$  versus magnetic field is shown in Fig. 5(c). Within  $B = 0.14\text{--}0.18$  T, where consistent locking was observed, a clear correlation existed between changes in the magnetic field and changes in the phase difference. This provides clear evidence for the modulated electron beam as the plausible locking mechanism, where the SBO locked to the second harmonic content of the LBO-modulated electron beam. Within the region that produced the highest powers, the standard deviation of the set of representative phase differences  $\overline{\Delta\phi}$  was  $17^\circ$ , which exceeds the accepted criterion of  $\pm 10^\circ$  for phase locking [10]. Thus, the harmonic frequency locking cannot be strictly described as phase locking. However, the phase difference between the SWSs was clearly not random, as would be the case for simple frequency locking. The mean phase variation  $\overline{\sigma_{\Delta\phi}}$  for shots in the region of optimal operation was  $8^\circ$ . As a proxy for the locking duration, the mean processing window width was found to be 17 ns. Table IV summarizes these results from the phase analysis.

## V. CONCLUSION

Experiments conducted using the MFRPM revealed the existence of a harmonic frequency-locked state after correcting

for axial magnetic field asymmetries. The locked state was characterized by low shot-to-shot variability and simultaneous peak power production by both SWSs. A phase analysis of the locked state showed that the shot-to-shot variation in the phase difference was slightly greater than the accepted standard for phase locking. However, the clear correlation between changes in the magnetic field and changes in the phase difference suggested the locking mechanism occurred through the electron beam. It is therefore plausible that the locking was facilitated by the second harmonic content of the 1-GHz modulated electron beam as it exited the LBO and entered the SBO. Experiments are being designed to investigate this locking phenomenon in a controlled manner.

## REFERENCES

- [1] G. B. Collins, Ed., *Microwave Magnetrons*. New York, NY, USA: McGraw-Hill, 1948.
- [2] R. J. Barker, J. H. Booske, J. H. Booske, and G. S. Nusinovich, Eds., *Modern Microwave and Millimeter-Wave Power Electronics*, 1st ed. Piscataway, NJ, USA: Wiley, 2005.
- [3] N. Friedman, *The Naval Institute Guide to World Naval Weapon Systems*, 5th ed. Annapolis, MD, USA: Naval Inst. Press, 2006.
- [4] A. Palevsky and G. Bekefi, "Microwave emission from pulsed, relativistic e-beam diodes. II. The multiresonator magnetron," *Phys. Fluids*, vol. 22, no. 5, pp. 986–996, 1979. [Online]. Available: <http://dx.doi.org/10.1063/1.862663>
- [5] J. Benford, H. Sze, T. Young, D. Bromley, and G. Proulx, "Variations on the relativistic magnetron," *IEEE Trans. Plasma Sci.*, vol. 13, no. 6, pp. 538–544, Dec. 1985. [Online]. Available: <http://dx.doi.org/10.1109/TPS.1985.4316470>
- [6] C. Leach, S. Prasad, M. I. Fuks, J. Buchenauer, J. W. McConaha, and E. Schamiloglu, "Experimental demonstration of a high-efficiency relativistic magnetron with diffraction output with spherical cathode end-cap," *IEEE Trans. Plasma Sci.*, vol. 45, no. 2, pp. 282–288, Feb. 2017. [Online]. Available: <http://doi.org/10.1109/TPS.2016.2644625>
- [7] J. S. Levine, B. D. Harteneck, and H. D. Price, "Frequency-agile relativistic magnetrons," *Proc. SPIE*, vol. 2557, pp. 74–80, Sep. 1995. [Online]. Available: <http://dx.doi.org/10.1117/12.218536>
- [8] A. S. Gilmour, *Klystrons, Traveling Wave Tubes, Magnetrons, Cross-Field Amplifiers, and Gyrotrons*. Boston, MA, USA: Artech House, 2011.
- [9] T. A. Treado, W. O. Doggett, G. E. Thomas, R. S. Smith, III, J. Jackson-Ford, and D. J. Jenkins, "Operating modes of relativistic rising-sun and A6 magnetrons," *IEEE Trans. Plasma Sci.*, vol. 16, no. 2, pp. 237–248, Apr. 1988. [Online]. Available: <http://dx.doi.org/10.1109/27.3820>
- [10] J. Benford, H. Sze, W. Woo, R. R. Smith, and B. Harteneck, "Phase locking of relativistic magnetrons," *Phys. Rev. Lett.*, vol. 62, no. 8, pp. 969–971, Feb. 1989. [Online]. Available: <http://dx.doi.org/10.1103/PhysRevLett.62.969>
- [11] S. C. Chen, "Growth and frequency pushing effects in relativistic magnetron phase-locking," *IEEE Trans. Plasma Sci.*, vol. 18, no. 3, pp. 570–576, Jun. 1990. [Online]. Available: <http://dx.doi.org/10.1109/27.55928>
- [12] T. A. Treado, P. D. Brown, and D. Aiguier, "New experimental results at long pulse and high repetition rate, from Varian's phase-locked magnetron array program," *Proc. SPIE*, vol. 1872, pp. 241–252, Jul. 1993. [Online]. Available: <http://dx.doi.org/10.1117/12.147464>
- [13] P. Pengvanich *et al.*, "Modeling and experimental studies of magnetron injection locking," *J. Appl. Phys.*, vol. 98, no. 11, p. 114903, Dec. 2005. [Online]. Available: <http://dx.doi.org/10.1063/1.2132513>
- [14] R. M. Gilgenbach, Y. Y. Lau, H. McDowell, K. L. Cartwright, and T. A. Spencer, "Crossed-field devices," in *Modern Microwave and Millimeter-Wave Power Electronics*, 1st ed., R. J. Barker, J. H. Booske, N. C. Luhmann, and G. S. Nusinovich, Eds. Piscataway, NJ, USA: Wiley-IEEE Press, 2005, pp. 289–342.
- [15] P. Pengvanich, Y. Y. Lau, E. Cruz, R. M. Gilgenbach, B. Hoff, and J. W. Luginsland, "Analysis of peer-to-peer locking of magnetrons," *Phys. Plasmas*, vol. 15, no. 10, p. 103104, 2008. [Online]. Available: <http://dx.doi.org/10.1063/1.2992526>

- [16] E. J. Cruz, B. W. Hoff, P. Pengvanich, Y. Y. Lau, R. M. Gilgenbach, and J. W. Luginsland, "Experiments on peer-to-peer locking of magnetrons," *Appl. Phys. Lett.*, vol. 95, no. 19, p. 191503, Nov. 2009. [Online]. Available: <http://dx.doi.org/10.1063/1.3262970>
- [17] G. B. Greening, N. M. Jordan, S. C. Exelby, D. H. Simon, Y. Y. Lau, and R. M. Gilgenbach, "Multi-frequency recirculating planar magnetrons," *Appl. Phys. Lett.*, vol. 109, no. 7, p. 074101, 2016. [Online]. Available: <http://dx.doi.org/10.1063/1.4961070>
- [18] R. M. Gilgenbach, Y.-Y. Lau, D. M. French, B. W. Hoff, J. Luginsland, and M. Franzi, "Crossed field device," U.S. Patent 8841867 B2, Sep. 23, 2014.
- [19] M. A. Franzi *et al.*, "Recirculating-planar-magnetron simulations and experiment," *IEEE Trans. Plasma Sci.*, vol. 41, no. 4, pp. 639–645, Apr. 2013. [Online]. Available: <https://doi.org/10.1109/TPS.2013.2242493>
- [20] M. A. Franzi *et al.*, "Microwave power and phase measurements on a recirculating planar magnetron," *IEEE Trans. Plasma Sci.*, vol. 43, no. 5, pp. 1675–1682, May 2015. [Online]. Available: <https://doi.org/10.1109/TPS.2015.2417774>
- [21] N. M. Jordan, G. B. Greening, B. W. Hoff, S. S. Maestas, S. C. Exelby, and R. M. Gilgenbach, "Additively manufactured high power microwave anodes," *IEEE Trans. Plasma Sci.*, vol. 44, no. 8, pp. 1258–1264, Aug. 2016. [Online]. Available: <http://dx.doi.org/10.1109/TPS.2016.2565261>
- [22] G. B. Greening, J. M. Nicholas, S. C. Exelby, Simon, H. David, Y. Y. Lau, R. M. Gilgenbach, "Multi-frequency recirculating planar magnetrons," Ph.D. dissertation, Dept. Nucl. Eng. Radiol. Sci., Univ. Michigan, Ann Arbor, MI, USA, 2017. [Online]. Available: <https://deepblue.lib.umich.edu/handle/2027.42/138623>
- [23] M. Franzi, R. Gilgenbach, Y. Y. Lau, B. Hoff, G. Greening, and P. Zhang, "Passive mode control in the recirculating planar magnetron," *Phys. Plasmas*, vol. 20, no. 3, p. 033108, 2013. [Online]. Available: <http://dx.doi.org/10.1063/1.4794967>
- [24] Z. Cendes, "The development of HFSS," in *Proc. USNC-URSI Radio Sci. Meeting*, Jun./Jul. 2016, pp. 39–40. [Online]. Available: <http://doi.org/10.1109/USNC-URSI.2016.7588501>
- [25] B. Goplen, L. Ludeking, D. Smith, and G. Warren, "User-configurable MAGIC for electromagnetic PIC calculations," *Comput. Phys. Commun.*, vol. 87, nos. 1–2, pp. 54–86, May 1995. [Online]. Available: [https://doi.org/10.1016/0010-4655\(95\)00010-D](https://doi.org/10.1016/0010-4655(95)00010-D)
- [26] Y. Y. Lau, private communication, Jan. 2017.
- [27] M. Unser, A. Aldroubi, and M. Eden, "Polynomial spline signal approximations: Filter design and asymptotic equivalence with Shannon's sampling theorem," *IEEE Trans. Inf. Theory*, vol. 38, no. 1, pp. 95–103, Jan. 1992. [Online]. Available: <https://doi.org/10.1109/18.108253>
- [28] A. Reilly, G. Frazer, and B. Boashash, "Analytic signal generation-tips and traps," *IEEE Trans. Signal Process.*, vol. 42, no. 11, pp. 3241–3245, Nov. 1994.
- [29] W. J. Williams, "Cross Hilbert time-frequency distributions," in *Proc. SPIE*, vol. 3461, pp. 120–130, Oct. 1998. [Online]. Available: <http://dx.doi.org/10.1117/12.325673>



**Geoffrey B. Greening** (M'12) received the B.S.E., M.S.E., and Ph.D. degrees in nuclear engineering and radiological sciences (plasma option) from the University of Michigan (UM), Ann Arbor, MI, USA, in 2010, 2012, and 2017, respectively.

His doctoral research was performed in the Plasma, Pulsed Power, and Microwave Laboratory at UM under the joint mentorship of Professors R. Gilgenbach and Y. Y. Lau.

**Steven C. Exelby** (S'15), photograph and biography not available at the time of publication.



**Drew A. Packard** (S'17) received the B.S.E and M.S.E degrees in nuclear engineering and radiological sciences from the University of Michigan, Ann Arbor, MI, USA, in 2016 and 2017, respectively.

He is currently a Graduate Student performing research on high-power microwave devices for Professor Gilgenbach with the Plasma, Pulsed Power, and Microwave Laboratory. He has completed two internships at L-3 Communications, Electron Devices Division, San Carlos, CA, USA.



**Nicholas M. Jordan** (M'05) received the B.S.E., M.S.E., and Ph.D. (plasma option) degrees in nuclear engineering and radiological science from the University of Michigan (UM), Ann Arbor, MI, USA, in 2002, 2004, and 2008, respectively.

In 2013, he joined the Plasma, Pulsed Power, and Microwave Laboratory, UM, an Assistant Research Scientist. He was with Cybernet Systems, Ann Arbor, MI, USA.



**Y. Y. Lau** (M'98–SM'06–F'08) was born in Hong Kong. He received the B.S., M.S., and Ph.D. degrees in electrical engineering from the Massachusetts Institute of Technology (MIT), Cambridge, MA, USA, in 1968, 1970, and 1973, respectively.

Since 1992, he has been a Professor with the Applied Physics Program, Department of Nuclear Engineering and Radiological Sciences, University of Michigan, Ann Arbor, MI, USA.



**Ronald M. Gilgenbach** (LF'06) received the B.S. and M.S. degrees from the University of Wisconsin, Madison, WI, USA, in 1972 and 1973, respectively, and the Ph.D. degree in electrical engineering from Columbia University, New York, NY, USA, in 1978.

He is currently the Chair and a Chihro Kikuchi Collegiate Professor with the Nuclear Engineering and Radiological Sciences Department, University of Michigan, Ann Arbor, MI, USA.